Nonmetal-metal transition in Zn_n $(n=2-20)$ clusters

Jinlan Wang,[1,*] Guanghou Wang,[1] and Jijun Zhao[2,†]
[1]*National Laboratory of Solid State Microstructures and Department of Physics, Nanjing University, Nanjing 210093, People's Republic of China*
[2]*Department of Physics and Astronomy, University of North Carolina at Chapel Hill, Chapel Hill, North Carolina 27599, USA*
(Received 8 March 2003; published 9 July 2003)

By using density functional calculation with generalized gradient approximation, we have studied the structural and electronic properties of the zinc clusters. The lowest-energy structures of Zn_n $(n=2-20)$ clusters are determined. Three kinds of growth pathways are obtained in the small zinc clusters from Zn_4 to Zn_8 and tetrahedron-based structures have favorable energy. The zinc clusters with 7–16 atoms are semiconductorlike. A structural transition from low coordination cagelike to high coordination compact structures is obtained around Zn_{17}. The Zn_n clusters with $n=4$, 7, 9, 10, 14, 18, 20 show relatively high stability, consistent with the electron shell model and mass spectra. The ionization potentials of the Zn_n clusters are calculated and compared with conducting sphere droplet model. The size evolution of zinc clusters from van der Waals to covalent and bulk metallic behavior is discussed. The Zn clusters show stronger metallicity than the Cd and Hg clusters with same size.

DOI: 10.1103/PhysRevA.68.013201 PACS number(s): 36.40.Cg, 36.40.Mr

I. INTRODUCTION

The transition from van der Waals to covalent and finally metallic bonding in the clusters of group 12 elements (Zn, Cd, and Hg) is an interesting topic in cluster physics [1–15]. Since the group 12 atoms have s^2 closed-shell atomic configuration like the helium, their dimers are van der Waals-like. However, the bulk phase of Zn, Cd, and Hg are all metallic because of the overlap between the *s* and *p* bands. Among the clusters of group 12 elements, most available experimental and theoretical studies are on the Hg_n clusters [6–10,15], while there are also some works on Cd_n [2–5]. The knowledge on zinc clusters is most limited so far. Experimental studies on zinc clusters beyond Zn_2 dimer have only been done with mass spectra [26]. There are a few *ab initio* calculations on small zinc clusters with up to six atoms [13]. Therefore, first principle calculations on Zn_n clusters up to larger size are essential to illustrate the size-dependent transition from van der Waals to covalent and metallic. It is also interesting to compare the nonmetal-metal transition behavior of Zn clusters with those of Cd and Hg, since the bulk Zn shows stronger metallicity than Cd and Hg.

II. METHOD

In this paper, we perform density functional calculations on Zn_n $(n=2-20)$ clusters by using the DMOL package [16]. The effective core potential and a double numerical basis including *d*-polarization function are chosen. The density functional is treated by the generalized gradient approximation (GGA) and the exchange-correlation potential parametrized by Perdew and Wang [17] is used. Self-consistent field electronic structure calculations are done with a convergence criterion of 10^{-5} a.u. on the total energy and electron density. Geometry optimizations are performed using the Broyden-Fletcher-Goldfarb-Shanno algorithm, with a convergence criterion of 10^{-3} a.u on the gradient and displacement. The current scheme gives an atomic ionization potential as 9.9 eV and bulk cohesive energy as 0.88 eV/atom for Zn atom, in reasonable agreement with the experimental value 9.39 eV and 1.35 eV, respectively. To obtain the global minimum structure of zinc clusters, we use a combination technique of empirical genetic algorithm search of structural isomers [18–20] and GGA local optimization. Gupta-like many-body potential is used in the empirical simulations [21]. As shown in previous works, such approach provides an efficient way to locate the lowest-energy structures of atomic clusters at accuracy level of GGA [5,22,23].

III. RESULTS AND DISCUSSION

In Table I, we compare the present GGA results with previous high-level quantum chemistry calculations using coupled-clusters (CC) method [13] from Zn_2 to Zn_6. It is known that density functional calculations cannot describe the van der Waals interactions well. Thus, it is not surprising to find certain great differences between the GGA and the CC calculations for smallest clusters Zn_2 and Zn_3. For Zn_2, the binding energy and bond length are 0.027 eV and 3.37 Å in current GGA calculation, while they are only 0.012 eV and 3.96 Å in CC calculation, respectively. For Zn_3, we find an equilateral triangle structure with bond length 3.08 Å at GGA level, while it is 3.75 Å in CC calculation. However, for larger clusters with more than four atoms, the discrepancy is becoming small and reasonably down to 10% between DF-GGA and CC results. These results demonstrate that the present method cannot treat van der Waals interactions well for smallest clusters. As the cluster becomes larger, the bonding in clusters will become more covalent or

*Mailing address: Chemistry Division, Argonne National Laboratory, Argonne, IL 60439, USA. Email: jlwang@anl.gov
†Present address: Institute for Shock Physics, Washington State University, Pullman, WA 99164, USA. Email: jzhao@wsu.edu

TABLE I. Bond lengths r, binding energies per atom E_b, vertical ionization potentials IP (eV), and vibrational frequencies ω (cm^{-1}), compared with coupled-cluster results and experimental data on Zn_2 dimer [13].

			Zn_2, chain ($D_{\infty h}$)		
	r (Å)	E_b/n (eV)	IP (eV)		ω (cm^{-1})
GGA	3.37	0.027	8.24		43.1
CC	3.96	0.012			22
expt.		0.017			26
			Zn_3, triangle (C_{3v})		
	r (Å)	E_b/n (eV)	IP (eV)		ω (cm^{-1})
GGA	3.08	0.073	7.97		59.9
CC	3.75	0.030	8.25		28.2
			Zn_4, tetrahedron (T_d)		
	r (Å)	E_b/n (eV)	IP (eV)		ω (cm^{-1})
GGA	2.84	0.172	7.98		94.5
CC	2.94	0.097	7.77		81.2
			Zn_5, trigonal bipyramid (D_{3h})		
	r_1 (Å)	r_2 (Å)	E_b/n (eV)	IP (eV)	ω (cm^{-1})
GGA	2.78	3.10	0.172	7.37	61.5
CC	2.89	3.25	0.100	7.29	58.6
			Zn_6, octahedron (O_h)		
	r (Å)	E_b/n (eV)	IP (eV)		ω (cm^{-1})
GGA	3.25	0.119	7.09		34.0
CC	3.60	0.063	7.32		27.4
			Zn_6, trigonal bipyramid (C_{2v})		
	r_1 (Å)	r_2 (Å)	E_b/n (eV)	IP (eV)	ω (cm^{-1})
GGA	3.00	3.10	0.175	6.98	
CC	3.03	3.55	0.101	7.13	

even metallic. Hence the GGA calculations are expected to describe the cluster properties to a satisfactory extent.

The lowest-energy structure and their metastable configurations of Zn_n clusters up to $n=8$ are plotted in Fig. 1. For the clusters larger than three atoms, three-dimensional (3D) configurations are preferred. For example, in the case of Zn_4, tetrahedron structure ($4a$) with bond length 2.84 Å is more stable than a planar rhombus ($4b$) with energy $\Delta E = 0.089$ eV. The lowest-energy structure for Zn_5 is a trigonal bipyramid ($5a$) that has lower energy than a square pyramid ($5b$, $\Delta E = 0.056$ eV) and "W-shaped" planar structure ($5c$, $\Delta E = 0.075$ eV). The compact structures found for Zn_3 to Zn_5 are the same as those for ground-state configurations of noble gas clusters [25], implying the nature of van der Waals-like bonding in these smallest zinc clusters.

In the case of Zn_6, trigonal bipyramid ($6a$) is lower in energy than octahedron ($6b, \Delta E = 0.057$ eV) and distorted planar triangle with D_{3h} symmetry ($6c, \Delta E = 0.059$ eV). As for Zn_7, the pentagonal bipyramid ($7b$) is not obtained as ground-state structure, while trigonal bipyramid ($7a$) is found to be more stable by $\Delta E = 0.014$ eV, and a face-capped pentagonal bipyramid ($7c$) is a local minima. For Zn_8, although little energy difference is found among the isomers, the capped pentagonal bipyramid ($8a$) has favorable energy compared with three-capped octahedron ($8b, \Delta E = 0.003$ eV) and a capped trigonal bipyramid ($8c, \Delta E = 0.007$ eV). Similar lowest-energy structure was found in Ge_8 cluster [23], implying the appearance of covalent bond around Zn_8 cluster.

Combined the above discussion and Fig. 1, three kinds of growth pathways are derived in the small cluster size range from Zn_4 to Zn_8. One is based on the tetrahedron structure ($4a$), that is, $4a \rightarrow 5a \rightarrow 6a \rightarrow 7a \rightarrow 8c$. This growth pathway represents the lowest energy structures up to the size of seven atoms. Then it is replaced by pentagon-based structure in Zn_8. The second growth pathway is based on planar rhombus and represents the trend of planarlike structure, that is, $4b \rightarrow 5c \rightarrow 6c \rightarrow 7c$. The obtained structures through this pathway correspond to higher energy and are less stable. Meanwhile, starting from the planar rhombus, another growth pathway, $4b \rightarrow 5b \rightarrow 6b \rightarrow 7b$, is found to be more stable than the planarlike structures. This also infers that

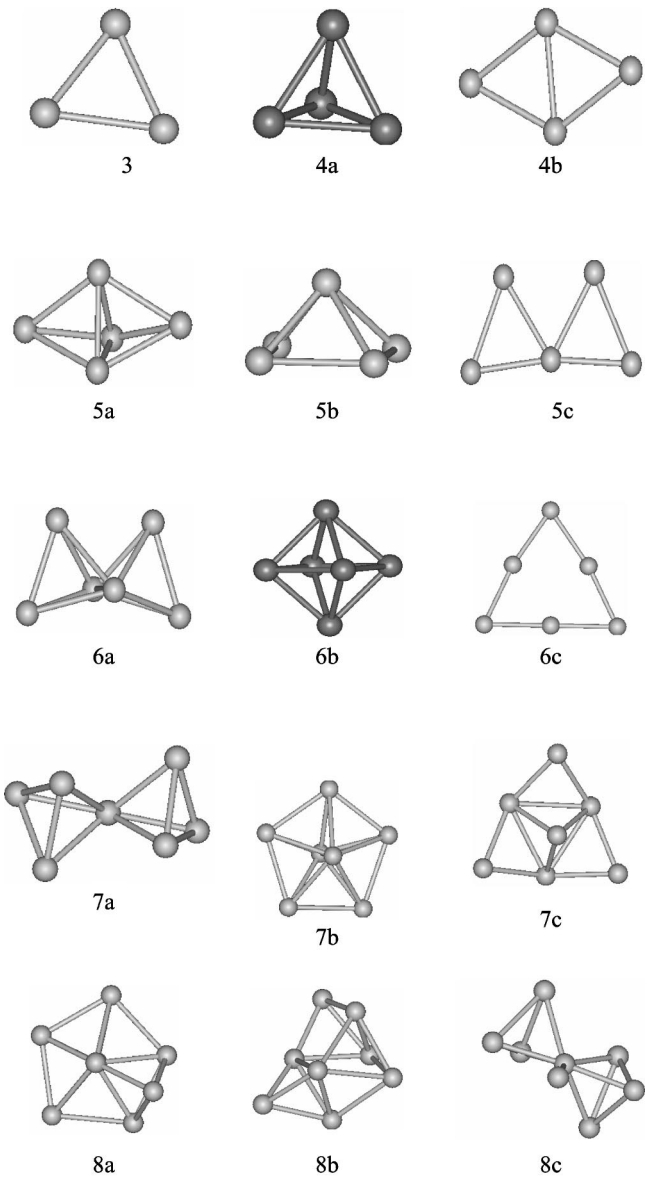

FIG. 1. The lowest-energy and metastable structures for small Zn_n clusters: $n=3-8$.

three-dimensional configuration is more stable than planar structure even in small zinc clusters.

In Fig. 2, we present the lowest-energy structure and some isomer for larger Zn_n clusters with $n=9-20$. For Zn_9, we find a tricapped trigonal prism (TTP) as ground-state structure, while the bicapped pentagonal bipyramid is nearly energetically degenerate ($\Delta E=0.0004$ eV). The latter one has been predicted as lowest-energy structure of Ge_9 clusters [23]. The Zn_{10} and Zn_{11} are square antiprism with C_{3v} symmetry and tricapped square antiprism, which can be obtained by one or two atoms capped on TTP Zn_9, respectively. Similarly, the lowest-energy structures in our calculations for Zn_{12} and Zn_{13} can also be seen as distorted Zn_9 plus three-capped and four-capped atoms. The favorable geometry for Zn_{14}, Zn_{15}, and Zn_{16} are layered structures based on two interpenetrating Zn_9 by minus or plus an atom, respectively. Therefore, the clusters with $n=10-16$ can be seen as growing from TTP Zn_9 subunit. These are very similar to the growth pattern of Ge_n clusters [23]. The similarity between Zn_n and Ge_n in the size range ($n=8-16$) implies that the Zn_n clusters are semiconductinglike. Such transition can be further supported by the *s-p* band gap (see Fig. 4), which will be discussed later. It is interesting to note that icosahedral structures is not found as the lowest-energy structrure for Zn_{13} cluster, while our previous GGA calculations have obtained icosahedron-based structures for Cd_{13-17} [5]. The icosahedron (13*b*) or cuboctahedron (13*c*) are all found as local minima for Zn_{13}, while icosahedron is more stable than cuboctahedron structure by $\Delta E=0.009$ eV. Similar results are found in the cluster Be_{13} [22] and Au_{13} [24] in our previous work.

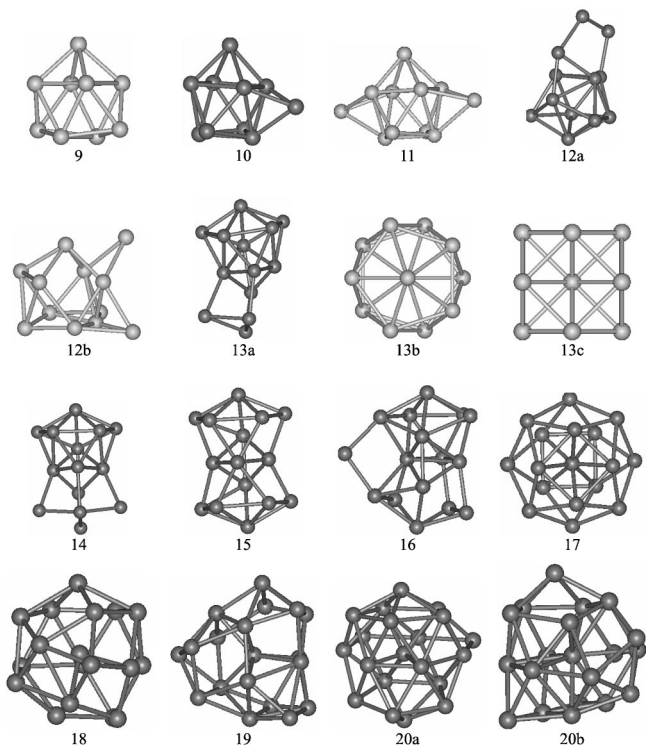

FIG. 2. The lowest-energy and metastable structures for medium-sized Zn_n clusters: $n=9-20$.

A structural transition from low coordination cagelike to high coordination compact structure is found around Zn_{17}. The most stable structure for Zn_{17} is ellipsoid comprising tetrahedral, pentagonal, and hexagonal subunits with one-atom center. The growth pattern continues for Zn_{18} and spherical structure is obtained as ground-state geometry. The characteristics is very similar to Be_{17-18} clusters [22], but different from Cd_{17-18} clusters [5] However, for Zn_{19}, TTP Zn_9 growth pattern appears again and can be viewed as three interpenetrating Zn_9 layered structure. Similar to Zn_{13}, the icosahedron or cuboctahedron is not the ground state structure for Zn_{19}. For Zn_{20}, layer-capped structure (20*a*) is found more stable than 20*b* by $\Delta E=0.047$ eV, while the latter one is predicted as lowest-energy structure for Cd_{20}. These results also indicate that the bonding in these Zn clusters is very different from van der Waals-like or covalent. The appearance of high-coordination compact structure

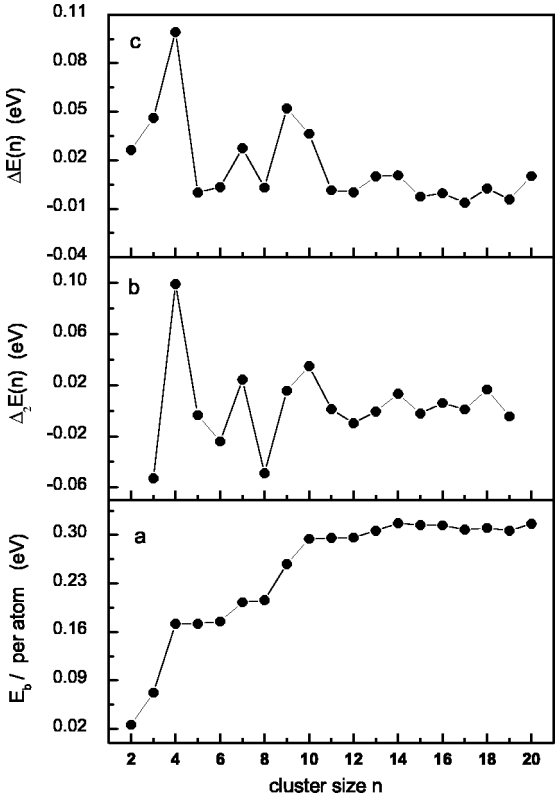

FIG. 3. Binding energy, second difference of binding energy, and fragment energy of Zn_n clusters as a function of cluster size n for $n=2-20$.

suggests that metallic cohesion becomes dominated in these clusters.

The binding energy E_b per atom of Zn_n cluster is described as a function of cluster size n in Fig. 3(a). Two sections of rapid increase in binding energy are found in the range of $n=2-4$ and $8-10$. The first one corresponds to the 2D to 3D transition and a significant decrease of bond length from 3.37 Å to 2.84 Å. Similar decreasing trend was also found in the small beryllium clusters [22]. The second pronounced increase comes from the transition from van der Waals to covalent bond. Therefore, the two steps ($4-7$, $10-16$) in Fig. 3(a) can be understood as van der Waal bonding and covalent bonding, respectively. On the contrary, although the transition from semiconductorlike to metallike bond is around Zn_{17}, the binding energy shows little change.

From above discussions, we can clearly see how the zinc clusters evolve from the molecular states to covalent and bulk metallic states as the size increases. In small zinc clusters, the 2*s* valence electrons are dominant in determining the cluster property. Since the electronic configuration of zinc atom ($4s^2$) is similar to helium, it is natural to understand that the small Zn_n ($n=2-6$) clusters exhibit certain noble gaslike behaviors. As the cluster size increases, the hybridizations of atomic orbitals, e.g., the hybridizations between the *s* states and unoccupied *p* states, lead to covalent bond nature in the clusters with $n=8-16$. The further hybridizations of orbitals may lead to the overlaps of the *s* states and *p* states and the metallization. The transition from covalent bonding to metallic bonding takes place around the size $n=17$.

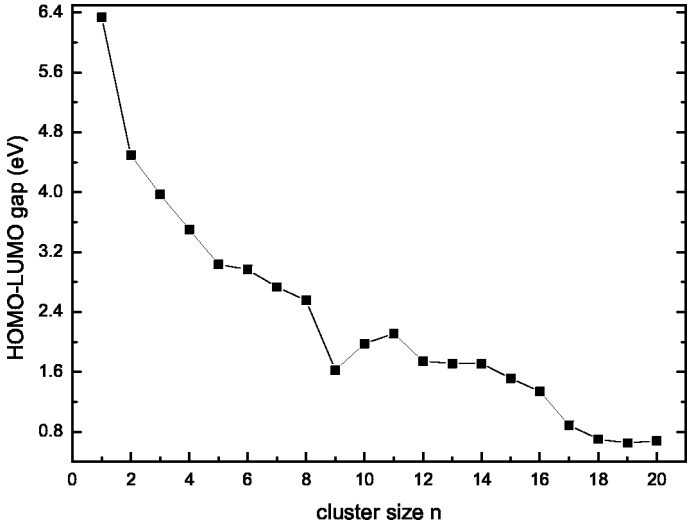

FIG. 4. HOMO-LUMO gaps of Zn_n clusters as a function of cluster size n for $n=2-20$.

To further illuminate the size-dependent transition of van der Waals to covalent and metallic cohesion on Zn clusters, we can examine the *s*-*p* band gap. As shown in Fig. 4, the gap between the highest occupied molecular orbital (HOMO) and lowest unoccupied molecular orbital (LUMO) of Zn_n clusters decreases rapidly from 4.59 eV for Zn_2 to 1.6 eV for Zn_9 and become smoothly decreasing afterwards up to 16. However, the decreasing trend is marked from 16 to 17 and becomes smooth again in the range of $18-20$. These may also support the point that the transitions from van der Waal to covalent bond and to metallic bond occur around 8 and 17, respectively. It is worthwhile to point out that the size dependence of HOMO-LUMO gap of Zn_n is different from those of divalent metal cluster Be_n, Cd_n, and Hg_n. The transition from van der Waals to covalent and metallic behavior in Zn_n is more rapid than that in Cd_n and Hg_n, but is slower than that in Be_n clusters. For example, the HOMO-LUMO gap of Zn_n clusters decreases from 4.59 eV for Zn_2 to 0.68 eV for Zn_{20}, while the band gaps for Be_2 and Be_{21} are 1.81 eV and 0.4 eV. However, the band gaps for Cd_2 and Cd_{21} are 3.94 eV and 0.86 eV and for Hg_3 and Hg_{20} are 3.43 eV and 1.8 eV, respectively.

Figures 3(b) and 3(c) give second difference of binding energy $\Delta_2E(n)=E(n+1)+E(n-1)-2E(n)$, and fragment energy $\Delta E(n)=E(n)-E(n-1)$ of Zn_n clusters as functions of cluster size. It is well known that $\Delta_2E(n)$ is a sensitive quantity that reflects the relative stability of clusters, while $\Delta E(n)$ describes the capability of losing an atom. Maxima are found at $n=4,7,9,10,14$ for $\Delta_2E(n)$, which may be understood by magic number of total valence electrons as 8,14,18,20,28 predicted by electronic shell model [2,3]. Similar electron shell effect has been found in other divalent metal clusters such as Cd_n, Be_n, and Hg_n clusters [5,15,22]. Different from other divalent metal clusters, Zn_{18} is found more stable than Zn_{17}. In experiments, mass spectra verify that the clusters with $n=10,18,20$ are the most stable ones

[26]. Fragment energy $\Delta E(n)$ also indicate that the clusters with $n=4,7,9,10,14,18,20$ are most stable compared to the neighbor clusters. However, fragment energy of Zn_9 is some higher than that of Zn_{10}, which may explain why the growth pathway of larger clusters Zn_{11-16} is on the basis of TTP Zn_9 instead of Zn_{10}.

The ionization potential is one of the most important quantities that can be used to signal the onset of metallic characteristics in the metal cluster. For alkali clusters such as Na_n, K_n, the IPs converge to its bulk limit (work function of solid) linearly with $n^{-1/3}$ (or $1/R$, R is the cluster radius) [3]. Such behavior can be modeled by a conducting spherical droplet (CSD) model [27,28], which considers the cluster as metallic spherical droplet and may even include some quantum effect correction [28]. For divalent metal cluster Hg_n [7], the $1/R$ law given by the CSD model is broken down below a certain critical cluster size, i.e, 20~50 atoms, corresponding to the nonmetallic behavior in those small clusters.

We calculate the vertical ionization potentials (IPs) from the total energy difference between the ground-state neutral Zn_n and the cationic Zn_n^+ clusters. In Fig. 5, the IPs of Zn_n are plotted as a function of $n^{-1/3}$ and compared along with the prediction of classical CSD model [28]. We find that the discrepancy of CSD model and theoretical values decreases rapidly as the cluster size increases. As n approaches 20, the discrepancy between density functional theory (DFT) calculations and CSD model becomes rather small, indicating that the Zn_n clusters with $n \geqslant 20$ become close to a metallic droplet. Relatively high ionization potentials are found in the clusters with $n=4,7,17,20$, which can be understood by the electronic shell model.

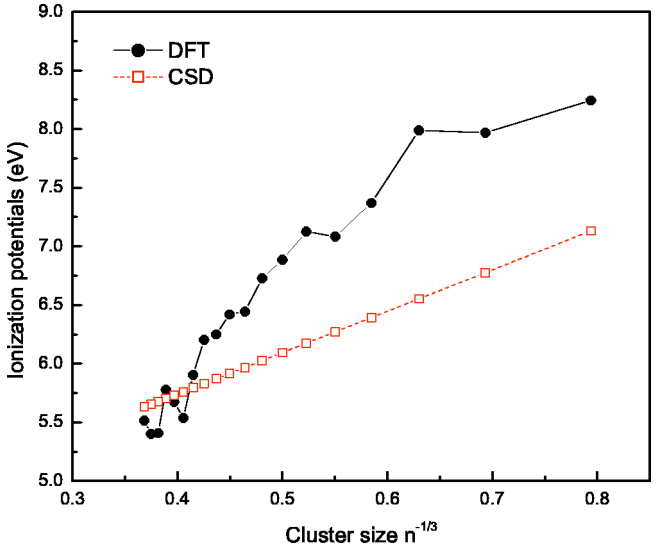

FIG. 5. Ionization potentials (IPs) vs cluster size n for Zn_n. Connected open circles: DFT calculations; dashed line: CSD model.

IV. CONCLUSION

In summary, we have studied the geometrical and electronic structures of zinc clusters by using GGA calculation combined with a genetic algorithm. The main conclusions can be made in the following points.

(1) Three kinds of growth pathways are obtained in the small cluster evolution with $n=4-8$.

(2) The transition from van der Waals to covalent bond happens around Zn_8, while the transition to metallic bond is around Zn_{17}.

(3) The binding energy, second difference of binding energy, fragment energy, and ionization potentials show that the clusters with $n=4,7,9,10,14,18,20$ are more stable than their neighboring clusters, corresponding to electronic shell model.

(4) The zinc clusters show more rapidly transition toward bulk metallicity than Cd and Hg clusters.

ACKNOWLEDGMENTS

This work was financially supported by the National Natural Science Foundation of China (No. 29890210) and the University Research Council of University of North Carolina at Chapel Hill. The authors acknowledge the computational support from Nanjing University and North Carolina Supercomputer Center.

[1] W.A. de Heer, Rev. Mod. Phys. **65**, 611 (1993).
[2] M. Ruppel and K. Rademann, Chem. Phys. Lett. **197**, 280 (1992); K. Rademann, M. Ruppel, and B. Kaiser, Ber. Bunsenges. Phys. Chem. **96**, 1204 (1992); K. Rademann, J. Non-Cryst. Solids **156-158**, 794 (1993).
[3] J. Zhao, X. Chen, and G. Wang, Europhys. Lett. **28**, 311 (1994).
[4] F. Yonezawa and H. Tanikawa, J. Non-Cryst. Solids **207**, 793 (1996).
[5] J.J. Zhao, Phys. Rev. A **64**, 043204 (2001).
[6] C. Brechignac, M. Broyer, Ph. Cahuzac, G. Delacretaz, P. Labastie, J.P. Wolf, and L. Woste, Phys. Rev. Lett. **60**, 275 (1988).
[7] K. Rademann, Z. Phys. D: At., Mol. Clusters **19**, 161 (1991); B. Kaiser and K. Rademann, Phys. Rev. Lett. **69**, 3204 (1992).
[8] K. Rademann, O. Dimopoulou-Rademann, M. Schlauf, U. Even, and F. Hensel, Phys. Rev. Lett. **69**, 3208 (1992).
[9] R. Busani, M. Folker, and O. Cheshnovsky, Phys. Rev. Lett. **81**, 3836 (1998).
[10] G.M. Pastor, P. Stampfli, and K.H. Bennemann, Europhys. Lett. **7**, 419 (1988).
[11] M. Dolg and H.J. Flad, Mol. Phys. **91**, 815 (1997).
[12] M. Yu and M. Dolg, Chem. Phys. Lett. **273**, 329 (1997).
[13] H.J. Flad, F. Schautz, Y. Wang, M. Dolg, and A. Savin, Eur. Phys. J. D **6**, 243 (1999).
[14] S. Park S, K. Lee K, and C. Lee, J. Korean Phys. Soc. **34**, 310 (1999).
[15] G.E. Moyano, R. Wesendrup, T. Sohnel, and P. Schwerdtfeger, Phys. Rev. Lett. **89**, 103401 (2002).
[16] DMOL is a density functional theory (DFT) package based

numerical atomic basis distributed by Accelrys Inc., B. Delley, J. Chem. Phys. **92**, 508 (1990).
[17] J.P. Perdew and Y. Wang, Phys. Rev. B **45**, 13 244 (1992).
[18] D.M. Deaven and K.M. Ho, Phys. Rev. Lett. **75**, 288 (1995); D.M. Deaven, N. Tit, J.R. Morris, and K.M. Ho, Chem. Phys. Lett. **256**, 195 (1996).
[19] Y.H. Luo, J.J. Zhao, S.T. Qiu, and G.H. Wang, Phys. Rev. B **59**, 14 903 (1999).
[20] J.J. Zhao, Y.H. Luo, and G.H. Wang, Eur. Phys. J. D **14**, 309 (2001).
[21] F. Cleri and V. Rosato, Phys. Rev. B **48**, 22 (1993).
[22] J.L. Wang, G.H. Wang, and J.J. Zhao, J. Phys.: Condens. Matter **13**, L753 (2001).
[23] J.L. Wang, G.H. Wang, and J.J. Zhao, Phys. Rev. B **64**, 205411 (2001).
[24] J.L. Wang, G.H. Wang, and J.J. Zhao, Phys. Rev. B **66**, 035418 (2002).
[25] *Clusters of Atoms and Molecules I*, edited by H. Haberland (Springer-Verlag, Berlin, 1995).
[26] I. Karakuse, T. Ichihara, Y. Fujita, M. Matsuo, T. Sakurai, and H. Matsuda, Int. J. Mass Spectrom. Ion Processes **69**, 109 (1986).
[27] D.M. Wood, Phys. Rev. Lett. **46**, 749 (1981).
[28] J.P. Perdew, Phys. Rev. B **37**, 6175 (1988).